

Diffusion Maps : Using the Semigroup Property for Parameter Tuning

Shan Shan and Ingrid Daubechies

March 8, 2022

Abstract

Diffusion maps (DM) constitute a classic dimension reduction technique, for data lying on or close to a (relatively) low-dimensional manifold embedded in a much larger dimensional space. The DM procedure consists in constructing a spectral parametrization for the manifold from simulated random walks or diffusion paths on the data set. However, DM is hard to tune in practice. In particular, the task to set a diffusion time t when constructing the diffusion kernel matrix is critical. We address this problem by using the semigroup property of the diffusion operator. We propose a semigroup criterion for picking the “right” value for t . Experiments show that this principled approach is effective and robust.

Keywords Diffusion maps Diffusion operator Semigroup properties Manifold learning Dimension reduction.

1 Introduction

Diffusion maps (DM) [4] are used in machine-learning to achieve dimension reduction for data that are assumed to be sampled from a lower-dimensional manifold within a higher-dimensional setting; they are related to other kernel eigenmap methods such as Laplacian eigenmaps [1], local linear embedding [10], Hessian eigenmaps [6] and local tangent space alignment [12].

The basic idea is simple: diffusion on a manifold is governed by the semigroup generated by the manifold’s Laplace-Beltrami operator; the spectral analysis of the diffusion operator thus provides information about the manifold that can be used to provide a lower-dimensional parametrization for the data that also removes “noise” from the data inconsistent with the manifold hypothesis. One can (approximately) simulate a random walk or diffusion process on the (unknown) manifold by taking small steps within the data set according to probabilities estimated from the distances between data points. Indeed, if the data points provide a sufficiently dense sampling of the manifold, then their distances (measured in the high-dimensional ambient space) within a close neighborhood of a fixed data point P are close approximations to the distances between the corresponding points within the pull-back of the neighborhood to the tangent plane at P ; the diffusion kernel on the manifold can be

likewise approximated (near P) by that on the tangent plane at P . Since the diffusion kernel in a Euclidean space takes the same form (up to normalization) regardless of the dimension, one can thus simply use the distances in the ambient large-dimensional Euclidean space to generate a reasonable approximation to the manifold diffusion kernel for short diffusion times.

More precisely, suppose we are given a set of points $\mathcal{D} = \{y_1, \dots, y_N\}$ residing in high-dimensional Euclidean space \mathbb{R}^K . To compute a low-dimensional representation of the data with DM, we first construct a diffusion kernel matrix $W^{(t)}$,

$$W_{ij}^{(t)} = \exp\left(-\frac{d^2(y_i, y_j)}{t}\right). \quad (1)$$

Here, $d(\cdot, \cdot)$ is a distance metric on \mathcal{D} , for example as defined by the L_2 norm $\|\cdot\|_2$ on \mathbb{R}^K , and t is a *diffusion time* parameter chosen by the user. (This parameter is the “short time” from the hand-waving argument in the preceding paragraph.) Further operations are typically carried out (see below) to correct for possible local differences in e.g. sampling density within the data set. The resulting discrete matrix is interpreted as an approximation to the diffusion kernel (i.e. the kernel of the semigroup generated by the Laplace-Beltrami operator) on the manifold assumed to underlie the data. The entries $(\Psi_\ell)_i$; $\ell = 1, \dots, L$, $i = 1, \dots, N$ (with $L \ll K$) of this matrix’s first few eigenvectors Ψ_ℓ , sometimes suitably weighted according to the eigenvalues λ_ℓ^t , then provide an L -dimensional parametrization for the data points y_i , $i = 1, \dots, N$.

This article is organized as follows. Section 2 gives a brief capsule description of the algorithm for computing diffusion maps and its mathematical interpretation. Section 3 discusses the sensitivity of the method to the choice for t , illustrates the difficulty in guesstimating the “right” t , and introduces the semigroup test as a criterion for determining a useful value for t ; we also give examples of using the semigroup test to the problems of finding optimal data embedding on synthetic data and real image data. Experiments show that this principled approach is effective and robust.

2 Diffusion operator and Diffusion maps: a brief recap

We present a very condensed summary; readers interested in more extensive discussion of Riemannian manifolds can consult e.g. [3]; the basics of Diffusion Maps can be found in [5].

2.1 Laplace Beltrami operator

We begin by defining the Laplace-Beltrami operator applied to a scalar function $f : \mathcal{M} \rightarrow \mathbb{R}$ on a Riemannian manifold \mathcal{M} ; for simplicity we shall assume \mathcal{M} to be compact, without boundary.

Definition (Laplace-Beltrami) Let \mathcal{M} be a Riemannian manifold with a metric g . The Laplace-Beltrami operator on \mathcal{M} is defined by

$$\Delta_{\mathcal{M}} f(x) = -\text{Trace} \nabla^{\mathcal{M}} \nabla f(x), \quad (2)$$

where $\nabla^{\mathcal{M}}$ denotes the canonical *Levi-Civita connection* on \mathcal{M} associated with g .

(In the case where \mathcal{M} is a compact manifold with a smooth boundary, one has to consider appropriate boundary conditions in order to define $\nabla_{\mathcal{M}}$ as a self-adjoint operator.)

The spectrum of $\Delta_{\mathcal{M}}$ on a compact manifold \mathcal{M} is discrete. Let the eigenvalues be $0 = \gamma_0 \leq \gamma_1 \leq \gamma_2 \leq \dots$ and let f_i be the eigenfunction corresponding to eigenvalue γ_i . Then the eigenfunctions of the Laplace-Beltrami operator give rise to an embedding operation with certain optimality properties.

An important observation (see e.g. [2]), is that $\|\nabla f\|$ provides us with an estimate of how far apart f maps nearby points. Let $y_i, y_j \in \mathcal{M}$; then

$$|f(y_i) - f(y_j)| \leq \text{dist}_{\mathcal{M}}(y_i, y_j) \|\nabla f\| + o(\text{dist}_{\mathcal{M}}(y_i, y_j)), \quad (3)$$

indicating that points close together on the manifold are mapped by f to values close together in \mathbb{R} . The extent to which f ‘‘preserves’’ locality can be measured by e.g.

$$\int_{\mathcal{M}} \|\nabla f(y)\|^2 d_{\text{vol}_{\mathcal{M}}} y; \quad (4)$$

minimizing this objective function is equivalent to finding eigenfunctions of the Laplace Beltrami operator $\Delta_{\mathcal{M}}$, in the following sense. The eigenfunction f_0 of $\Delta_{\mathcal{M}}$ with the lowest value for (4) is a constant function on $\Delta_{\mathcal{M}}$ (for which $\nabla f(y) = 0$ for all y), which is completely uninformative concerning localization of manifold points w.r.t. each other, since it maps all points to the same value in \mathbb{R} . The next eigenfunction f_1 provides an optimal embedding map to the real line (in the sense that it minimizes the integral over \mathcal{M} of the averaged distortion bound (4)); similarly, the optimal embedding of the manifold in \mathbb{R}^L is defined by

$$\mathbf{g} := (f_1(y), \dots, f_L(y)). \quad (5)$$

2.2 Diffusion operator

Although the first L eigenvectors of the Laplace-Beltrami operator provide an informative embedding of \mathcal{M} in \mathbb{R}^L , it can be difficult to identify these eigenvectors with a reasonable degree of accuracy, starting from noisy samples of \mathcal{M} . For this reason, it may be useful, in order to determine (approximations to) these eigenvectors, to work instead with the semigroup of operators $\{e^{-t\Delta_{\mathcal{M}}}\}_{t \geq 0}$. The Laplace-Beltrami operator $\Delta_{\mathcal{M}}$ is the infinitesimal generator of $e^{-t\Delta_{\mathcal{M}}}$, i.e.,

$$\lim_{t \rightarrow 0} \frac{I - e^{-t\Delta_{\mathcal{M}}}}{t} f = -\Delta_{\mathcal{M}} f, \quad (6)$$

whenever f belongs to a suitable dense subset of $C(\mathcal{M})$. The diffusion operators $\{e^{-t\Delta_{\mathcal{M}}}\}_{t > 0}$ share the same eigenfunctions as $\Delta_{\mathcal{M}}$, and the eigenvalues of $e^{-t\Delta_{\mathcal{M}}}$ are exactly the $e^{-\gamma_i t}$; in particular, they are bounded: $1 = e^{-\gamma_0 t} \geq e^{-\gamma_1 t} \geq e^{-\gamma_2 t} \geq \dots > 0$.

The Laplace-Beltrami operator $\Delta_{\mathcal{M}}$ and the diffusion operator $e^{-t\Delta_{\mathcal{M}}}$ are also related through the heat (or diffusion) equation on the manifold.

Definition (Heat Equation). Let $f : \mathcal{M} \rightarrow \mathbb{R}$ be the initial temperature distribution on a manifold \mathcal{M} embedded in \mathbb{R}^K . The *heat equation* is the partial differential equation

$$\begin{aligned} \frac{\partial u}{\partial t} + \Delta_{\mathcal{M}} u &= 0, \\ u(x, 0) &= f(x). \end{aligned} \quad (7)$$

The solution of the heat equation is given by the diffusion operator $e^{-t\Delta_{\mathcal{M}}}$,

$$u(x, t) = e^{-t\Delta_{\mathcal{M}}} f(x) \quad (8)$$

$$= \int_{\mathcal{M}} h_t(x, y) f(y) d_{\text{vol}_{\mathcal{M}}} y. \quad (9)$$

In the integral from (9), h_t is called the *heat kernel*. When x, y are close to each other and t is small, h_t can be approximated by the Gaussian

$$h_t(x, y) = (4\pi t)^{-\frac{d}{2}} e^{-\frac{\|x-y\|^2}{4t}}, \quad (10)$$

where d is the dimension of \mathcal{M} .

2.3 Approximating the diffusion operator on a discrete dataset

On discrete data samples of N data objects in K dimensions, interpreted as points of an unknown Riemannian manifold \mathcal{M} embedded in \mathbb{R}^K , an approximation of the diffusion operator $e^{-t\Delta_{\mathcal{M}}}$ is built as follows. First, define the N by N matrix W ,

$$W_{ij} = \begin{cases} e^{-\frac{\|y_i - y_j\|^2}{4t}} & \text{if } \|y_i - y_j\| < \epsilon \\ 0 & \text{otherwise} \end{cases} \quad (11)$$

where ϵ is picked in concordance with t ; typically ϵ is proportional to $(Ct)^{1/2}$ for some C significantly larger than 1; the W_{ij} set to zero thus correspond to entries that would otherwise be so small that they would not contribute much to the overall matrix, while setting them to zero alleviates the complexity of the algorithm. The action of the true diffusion kernel, acting as an integral operator on the constant function 1 on \mathcal{M} , would produce the function 1 again; the discrete approximation W typically does not have the same effect on the all-ones vector approximating the function 1. Many of the approximation ingredients contribute to this shortcoming, such as setting some of the W -entries to zero, or (more importantly) local variations in the data manifold sampling, which result in some data points having more and/or closer neighbors than others and which also cause the summing (rather than integration) procedure to deviate from an optimal quadrature. To remedy the total effect of these shortcomings to some extent, one defines a diagonal matrix $D = [D_{ii}]_{i=1}^N$, with entries given by $D_{ii} = \sum_j W_{ij}$; the matrix $D^{-1}W$ then does indeed map the all-ones vector to itself. (Note that this also neatly sidesteps the problem that we had no estimate for the dimension d of \mathcal{M} , which would, in principle, have been necessary for the normalization of the gaussian approximation to h_t .) We then compute eigenvalues and eigenvectors for $D^{-1}W$, i.e.

$$D^{-1}W\mathbf{f}_\ell = \lambda_\ell \mathbf{f}_\ell, \quad (12)$$

where we order the eigenvalues and eigenvectors so that $1 = \lambda_0 \geq \lambda_1 \geq \lambda_2 \geq \dots$. The k -dimensional embedding is then defined by

$$\mathbf{g}_i = (\mathbf{f}_1^{[i]}, \dots, \mathbf{f}_L^{[i]}), \quad (13)$$

where $\mathbf{f}_\ell^{[i]}$ is the i -th entry in the N -dimensional ℓ -th eigenvector.

Figure 1 illustrates this embedding on a simple example. The dataset consists of points residing on a helix wrapped around a torus, and shows the 2D embeddings obtained by Laplacian eigenmaps and diffusion maps, comparing them with those from PCA and MDS; Laplacian-based methods clearly do the better job recovering the intrinsic data structure – in this example, PCA and MDS essentially give results similar to a linear projection onto a 2D-plane.

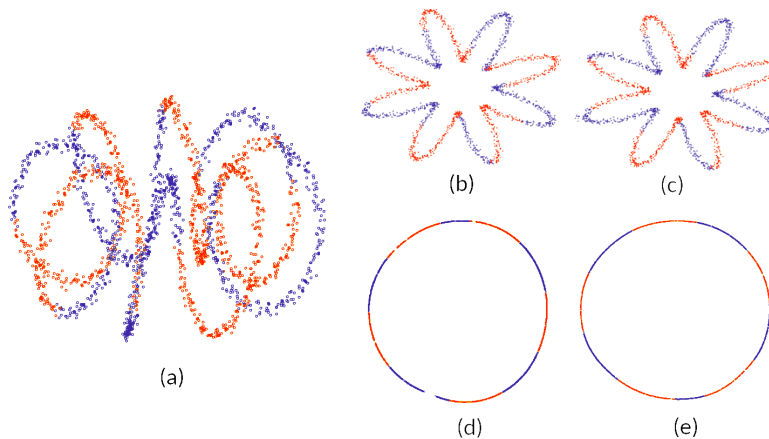


Figure 1: (a) Original data points, uniformly sampled (with some noise added) from a helicoidal curve wrapped around a torus in 3D. (We note that although we show the data embedded in a low-dimensional space in all our examples, the size of the ambient dimension has no impact on these methods, since they depend only on the distances between data points.)

Smaller panels: 2D embeddings of these data obtained via (b) PCA, (c) MDS, (d) Laplacian eigenmaps, and (e) Diffusion eigenmaps

In a second example the data are sampled uniformly (without added noise) from a 2D “Swiss roll” surface (a rectangle rolled up so that it forms a spiral – see Fig. 2(a)) embedded in 3D. Figure 2 compares the embeddings produced by Laplacian eigenmaps and by Diffusion maps, showing that Diffusion maps introduce fewer deformations.

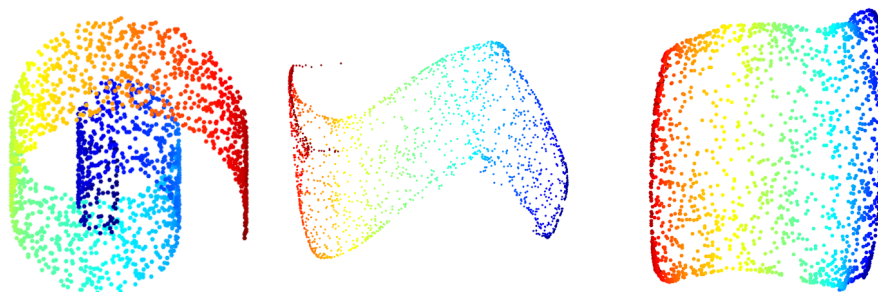


Figure 2: Left: original Swiss roll data; Middle and Right: 2D Embeddings obtained via Laplacian eigenmaps and Diffusion maps, respectively.

Remarks

1. The same “normalization by left-multiplication by a diagonal matrix” approach can be (and has been) used for the Laplace-Beltrami operator $\Delta_{\mathcal{M}}$ rather than $e^{-t\Delta_{\mathcal{M}}}$; approximating the differential operator by a matrix L expressing a second-order difference, and then “normalizing” it by setting $D^{-1}L$, leads to the Laplacian eigenmaps proposed in [2].
2. Although the matrix W is symmetric, the “normalized” version $D^{-1}W$ typically isn’t. One can also consider instead the symmetrized version $D^{-1/2}WD^{-1/2}$, which has the same eigenvalues as $D^{-1}W$; its eigenvectors are the vectors $D^{1/2}\mathbf{f}_{\ell}$.
3. In case the sampling density is known to be systematically not uniform over the manifold, it can be useful to introduce a correction for this in the matrix construction. The paper [4] describes in detail how one can modify the construction to incorporate (an approximation to) the sampling density. Depending on the value assigned to a tuning parameter α , the modification introduced in [4] can be interpreted (when $\alpha = 1$) as introducing a Jacobian-like factor (so that, in the limit for finer and finer sampling, one recovers again the standard diffusion semi-group and its Laplace-Beltrami generator), or (when $\alpha \neq 1$) as an adjustment of the diffusion process itself, with a non-constant diffusivity; in the latter case, the approximation is linked to a different semigroup, the eigenvectors and eigenvalues of which encode again significant geometric information about the manifold, and can therefore again be used for a lower-dimensional parametrization of the manifold.

3 Setting the diffusion time t

3.1 Sensitivity to the choice of t

It is intuitively clear that the algorithm described earlier can work only in some window for t : if t is chosen very large, then W_{ij} will be different from zero even for pairs i, j for which the data points y_i and y_j are far from each other in the ambient space, although we expect that their Euclidean distance is not at all informative about their relative roles on the manifold \mathcal{M} . We argued in Section 2 that the construction of $(W_t)_{ij}$ (where we now explicitly denote the dependence of W on t) was reasonable for i, j where the distance $\|y_i - y_j\|$ was sufficiently small that y_j could be viewed as close to the tangent plane to \mathcal{M} at y_i ; this means we should expect the method to work well only for t below some threshold. This is also consistent with the proofs in [5] and [4]: since those are proofs holding for $t \rightarrow 0$, the similarity of the eigendecompositions of W_t and the true diffusion operator $e^{-t\Delta_{\mathcal{M}}}$ on \mathcal{M} can be expected only in the regime of small t .

When t is too small, the method faces a different problem: for $t < \min_{i \neq j} \|y_i - y_j\|^2$, W reduces to the identity operator, and no useful embedding can be constructed. The problem persists for slightly larger values of t , where only a few (i, j) emerge above the threshold. In a certain sense, the diffusion time is then too short for the diffusion process to consistently bridge the distance between sample points on \mathcal{M} . Ideally, one would like that for each i , $(W_t)_{ij} \neq 0$ for several $j \neq i$. (One would also like the number of such “useful” neighbors not to vary by orders of magnitude over the dataset. This is possible only if the sampling is fairly uniform. It is when the spatial distribution of the points in the dataset varies so much that no

single parameter setting in the definition of W_t allows for the number $\#\{j \neq i; (W_t)_{ij} \neq 0\}$ to be at least (say) 10 for all i without getting into the several 100s for other i , that it is necessary to adapt the simple diffusion operator W_t , e.g. using the methods in [4].)

Finding the “right” choice for t , in the happy medium between the two extreme regimes, can be tricky: as illustrated in Figures 3 and 4 below, different choices for t can lead to very different outcomes for the same data.

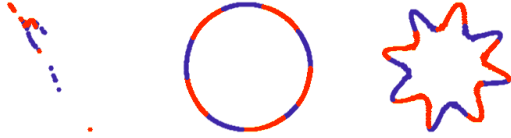


Figure 3: Three embeddings of the helicoidal data from Figure 1 obtained via Diffusion maps, for different choices for the parameter t : t_1 (left), t_2 (middle) and t_3 (right). The choice $t = t_2$ was adopted for Fig.1(e); the choices $t = t_1 = t_2/16$ and $t = t_3 = 4t_2$ are clearly suboptimal.

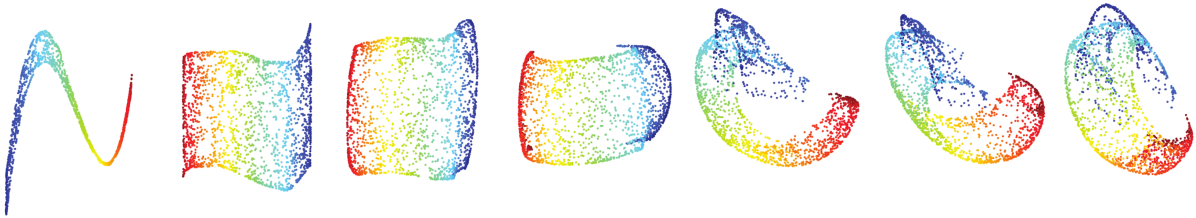


Figure 4: Several embeddings of the Swiss roll data from Fig. 2 obtained by the Diffusion map procedure of Section 2; the only difference lies in the choice of the parameter t , increasing from left to right in the figure by a factor 2 each time.

3.2 Semigroup test

In practical applications of Diffusion maps, it can take quite a bit of trial and error to find a “right” value for t . Our goal here is to describe a simple robust guiding strategy to reduce this guesswork, which finds a near-optimal value for t in many situations in which we have tested it.

The diffusion operators $\{e^{-t\Delta_{\mathcal{M}}}\}_{t>0}$ form a strongly continuous semigroup; i.e. the $T_t := e^{-t\Delta_{\mathcal{M}}}$ satisfy

$$T_{t_1+t_2} = T_{t_1}T_{t_2}, \quad \text{and } s\text{-}\lim_{t \rightarrow 0} T_t = \text{Id} . \quad (14)$$

It follows that the matrices $D_t^{-1}W_t$, used to define diffusion maps, or their symmetrized versions $K_t := D_t^{-1/2}W_tD_t^{-1/2}$, can be approximate, discretized versions of the diffusion operators on \mathcal{M} only when they likewise (approximately) satisfy the semigroup property.

We use this insight to formulate a criterion to pick an “optimal” t . In the regime where the K_t -operators are reasonable approximations of the semigroup $\{e^{-t\Delta_{\mathcal{M}}}\}_{t \geq 0}$, $(K_t)^2$ should be close to K_{2t} . This motivates the definition of the *semi-group error* (SGE)(t),

$$\text{SGE}(t) := \|(K_t)^2 - K_{2t}\|. \quad (15)$$

The norm used here is the operator norm; the operators we consider are (expected to be) positive, with eigenvalues between 0 and 1, and the range for $\text{SGE}(t)$ is between 0 and 1.

In practice, we begin with initializing a wide range of discrete values for t , i.e. we pick a set $T := \{t_m; m = 1, \dots, M\}$. For each t_m in T , we construct the diffusion matrices $(K_{t_m})^2$ and K_{2t_m} , and we compute $(\text{SGE})(t_m)$.

Figure 5 below plots the semi-group error $\text{SGE}(t)$ for different values of t for the Swiss roll example of Figures 2 and 4; $\text{SGE}(t)$ reaches its lowest value for the choice of t where the 2D-embedding is closest to a rectangle, which we know to be the ground truth in this case.

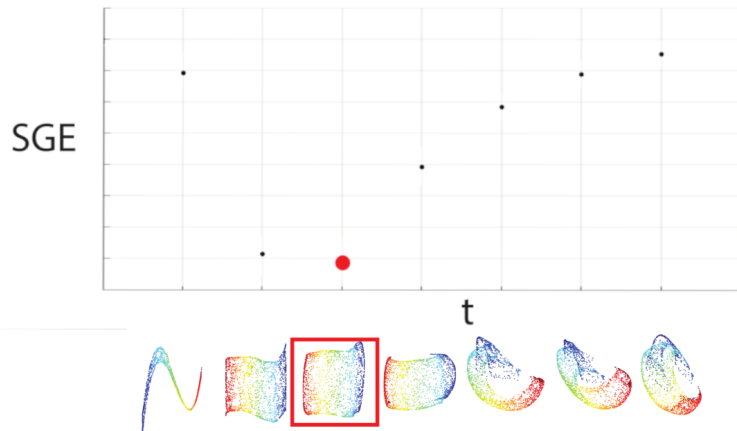


Figure 5: Semi-group error SGE for the Swiss roll data, for the values of t illustrated in Figure 3. The red dot is the optimal value of t , and corresponds to the embedding that visually best reflects the ground truth. The scale for t is logarithmic; each of the successive t_m (at the tick marks) is larger by factor 2 than the previous one, $t_{m+1} = 2t_m$.

In Figure 6, below, we revisit the three embeddings shown in Figure 3, next to the semi-group error plot for this dataset, and we observe that the visually optimal embedding (which is also the most accurate version of the ground truth for this manifold \mathcal{M}) corresponds again to the value of t with the smallest SGE in the regime of small diffusion times.

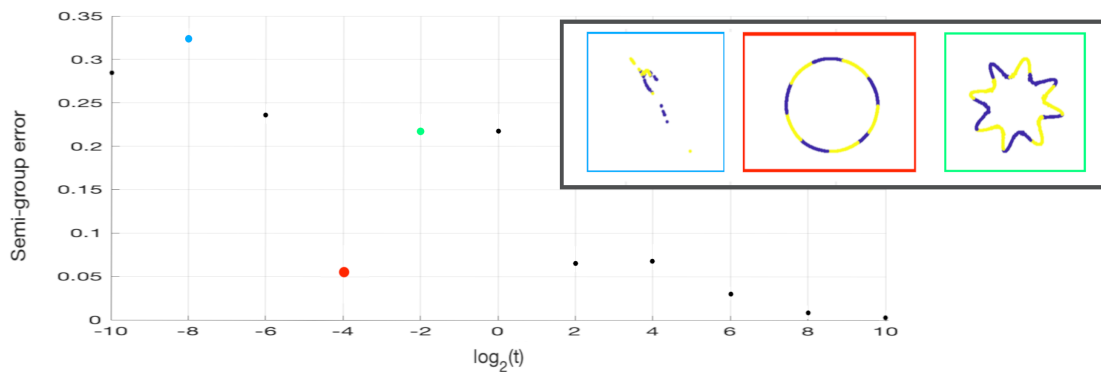


Figure 6: Semi-group error plot for a wide range of candidate values for t – the ratio t_{\max}/t_{\min} equals 2^{20} ! – for the dataset illustrated in Figures 1 and 3. Note that for very large t , the SGE estimate becomes small again – see discussion in the text.

As shown in Figure 6, the values of $\text{SGE}(t)$ behave qualitatively as we would have expected, based on the intuition explained at the start of this section: when t is very small, the semigroup behavior of the K_t hasn't "kicked in" yet, because the numerical diffusion's range is too short, and this is reflected by larger values for $\text{SGE}(t)$. (We recall that the range of SGE values is between 0 and 1; values exceeding .3 are indeed "large".) As t increases, $\text{SGE}(t)$ drops to lower values, to start increasing again after a minimum SGE-value not too far above 0. (These small values are maintained in an interval for t , as may not be evident from Figure 6, in which the successive values of t increase by a factor 4, $t_{m+1} = 4t_m$; detailed behavior in the neighborhood of each t_m is not apparent from this figure.) We interpret this increase as the influence of ambient-space geometry (such as the toroidal winding in this example), once the numerical diffusion is no longer "following" the manifold \mathcal{M} ; because even noisy sampling from \mathcal{M} translates to very non-uniform sampling in the higher-dimensional ambient space, the K_t are less close to following a semi-group behavior. When t increases further, the value of $\text{SGE}(t)$ starts decreasing again: once the reach of the numerical diffusion is sufficiently large that the "sources" on or near \mathcal{M} all "act" as one diffuse blob, and the geometry of \mathcal{M} has been obscured, the semigroup nature of the ambient-space diffusion takes over. Although $\text{SGE}(t)$ is small again, one cannot use these diffusion maps to generate an informative low-dimensional embedding of \mathcal{M} for t in this range.

We next turn to a few examples with non-uniform sampling. In this case we compensate for the change in sampling density by using the techniques described in [4], using an integral kernel $A_{t,\alpha}$ obtained by a "renormalization" of W_t . Regardless of the parameter setting for α that gives the best results (which depends on the type of non-uniformity), the basic intuition underlying the method remains the same: the spectral analysis, used to construct a low-dimensional embedding of \mathcal{M} , is predicated on the $A_{t,\alpha}$ approximating the kernels of a semigroup of operators. One can thus again use the SGE to determine optimal choices of t . Figure 7 shows the results for a non-uniformly sampled circle.

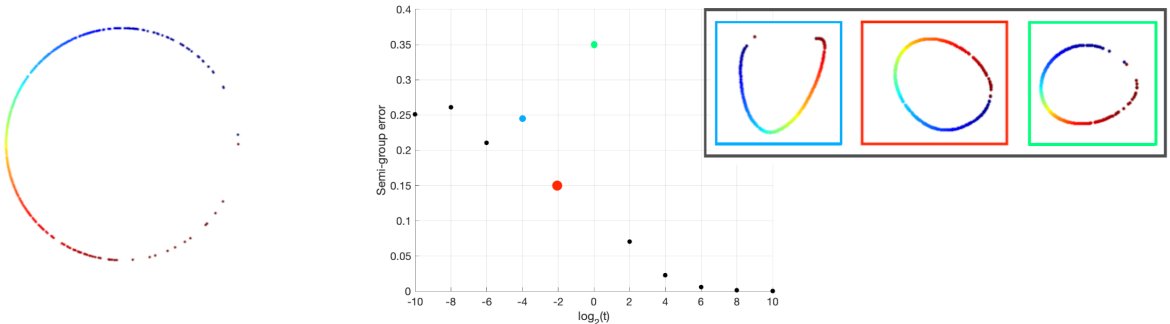


Figure 7: Left: 512 non-uniformly sampled points on a circle; Middle: $\text{SGE}(t)$ for a wide range of t values, with the useful-range optimal t marked in red; Upper right inset: the embeddings obtained for the optimal $t = 1/4$ and for $t = 1/16$ (left) and $t = 1$ (right). In this example, we set $\alpha = 2$ to determine the adapted kernels $A_{t,\alpha}$. (In this case, there is hardly any dimension reduction, since both the original and final circle are depicted on a 2D plane; this is a toy example, after all. It may be worth noting that the parametrization by Diffusion maps would have been identical had the data been embedded in a random not-coordinate-aligned plane in a much higher dimensional space.)

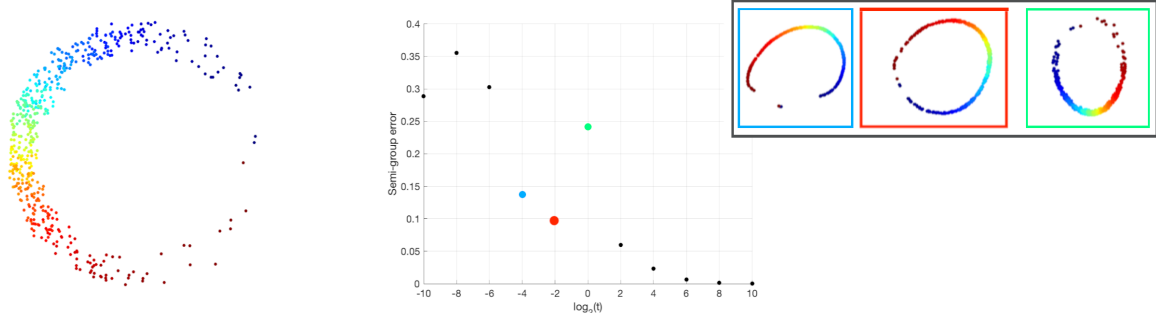


Figure 8: Left: 512 non-uniformly sampled points on a circle, now with noise added; Middle: $SGE(t)$ for a wide range of t values, with the useful-range optimal t marked in red; Upper right inset: the embeddings obtained for the optimal $t = 1/4$, as well as for $t = 1/16$ (left) and $t = 1$ (right). In this case, we have again set $\alpha = 2$ to determine the adapted kernels $A_{t,\alpha}$.

To illustrate the robustness of our the SGE test, we examine this dataset again after noise has been added. The results are shown in Figure 8.

After the simulated toy data examples, we conclude with one example of real data.

The dataset is part of the extended Yale Face Database B [7]; it consists of 64 images (192 pixels by 168 pixels) of the same human face, in the same pose, under different illumination conditions: the light source is moved around in two different directions. The intrinsic dimensionality of this collection of images is therefore expected to be 2, although the images themselves are objects in a much higher-dimensional space. We applied Diffusion maps, coupled with the semigroup-error tuning strategy described above, to this collection; the results are shown in Figure 9. By its very nature, the dataset in this example is noisy, since all photographs (as opposed to images generated by computer graphics) are inherently noisy, but we don't have an explicit characterization of this noise. To illustrate robustness of our analysis and semigroup criterion to noise, we resort to a common strategy in image analysis: we revisit the dataset in Figure 10, after extra noise has been added independently to each of the 64 images.

To add noise to the datapoints, from Figure 9 to Figure 10, we proceeded as follows. For each of the 192×168 pixels in each of the 64 images, we generated a random integer I uniformly in $[-100, 100]$; we then replaced the pixel value P by $P + I$ if $0 < P + I < 255$, by 0 if $P + I < 0$ or by 255 if $P + I > 255$. An example of one of the face photographs, before and after adding noise, is shown in Figure 11 below.

Despite the severity of the noise, we observe that the Diffusion Map analysis, combined with the semigroup tuning strategy, is remarkably robust: the same t_{opt} is selected in both cases, and the corresponding 2D embeddings are very similar (up to an inversion of the axis in one of the 2 variables), as illustrated by Figure 12 below.

4 Conclusion

Although Diffusion maps have shown to be a powerful tool to explore datasets embedded in high dimensions that are suspected to have interesting geometric structure on a much lower-dimensional scale [8][11][9], determining the “right” value for the diffusion parameter

t has been found to be tricky. Picking t so that it minimizes the Semi-Group Error is computationally easy, makes sense from a theoretical point of view, and gives good results in practice.

References

- [1] M. Belkin and P. Niyogi. Laplacian eigenmaps for dimensionality reduction and data representation. Neural computation, 15(6):1373–1396, 2003.
- [2] M. Belkin and P. Niyogi. Towards a theoretical foundation for laplacian-based manifold methods. Journal of Computer and System Sciences, 74(8):1289–1308, 2008.
- [3] W. M. Boothby and W. M. Boothby. An introduction to differentiable manifolds and Riemannian geometry, Revised, volume 120. Gulf Professional Publishing, 2003.
- [4] R. R. Coifman and S. Lafon. Diffusion maps. Applied and computational harmonic analysis, 21(1):5–30, 2006.
- [5] R. R. Coifman, S. Lafon, A. B. Lee, M. Maggioni, B. Nadler, F. Warner, and S. W. Zucker. Geometric diffusions as a tool for harmonic analysis and structure definition of data: Diffusion maps. Proceedings of the national academy of sciences, 102(21):7426–7431, 2005.
- [6] D. L. Donoho and C. Grimes. Hessian eigenmaps: Locally linear embedding techniques for high-dimensional data. Proceedings of the National Academy of Sciences, 100(10):5591–5596, 2003.
- [7] A. S. Georghiades, P. N. Belhumeur, and D. J. Kriegman. From few to many: Illumination cone models for face recognition under variable lighting and pose. IEEE transactions on pattern analysis and machine intelligence, 23(6):643–660, 2001.
- [8] J. Liu, Y. Yang, and M. Shah. Learning semantic visual vocabularies using diffusion distance. In 2009 IEEE Conference on Computer Vision and Pattern Recognition, pages 461–468. IEEE, 2009.
- [9] K. R. Moon, D. van Dijk, Z. Wang, S. Gigante, D. B. Burkhardt, W. S. Chen, K. Yim, A. v. d. Elzen, M. J. Hirn, R. R. Coifman, et al. Visualizing structure and transitions in high-dimensional biological data. Nature biotechnology, 37(12):1482–1492, 2019.
- [10] S. T. Roweis and L. K. Saul. Nonlinear dimensionality reduction by locally linear embedding. Science, 290(5500):2323–2326, 2000.
- [11] D. Van Dijk, R. Sharma, J. Nainys, K. Yim, P. Kathail, A. J. Carr, C. Burdziak, K. R. Moon, C. L. Chaffer, D. Pattabiraman, et al. Recovering gene interactions from single-cell data using data diffusion. Cell, 174(3):716–729, 2018.
- [12] T. Zhang, J. Yang, D. Zhao, and X. Ge. Linear local tangent space alignment and application to face recognition. Neurocomputing, 70(7-9):1547–1553, 2007.

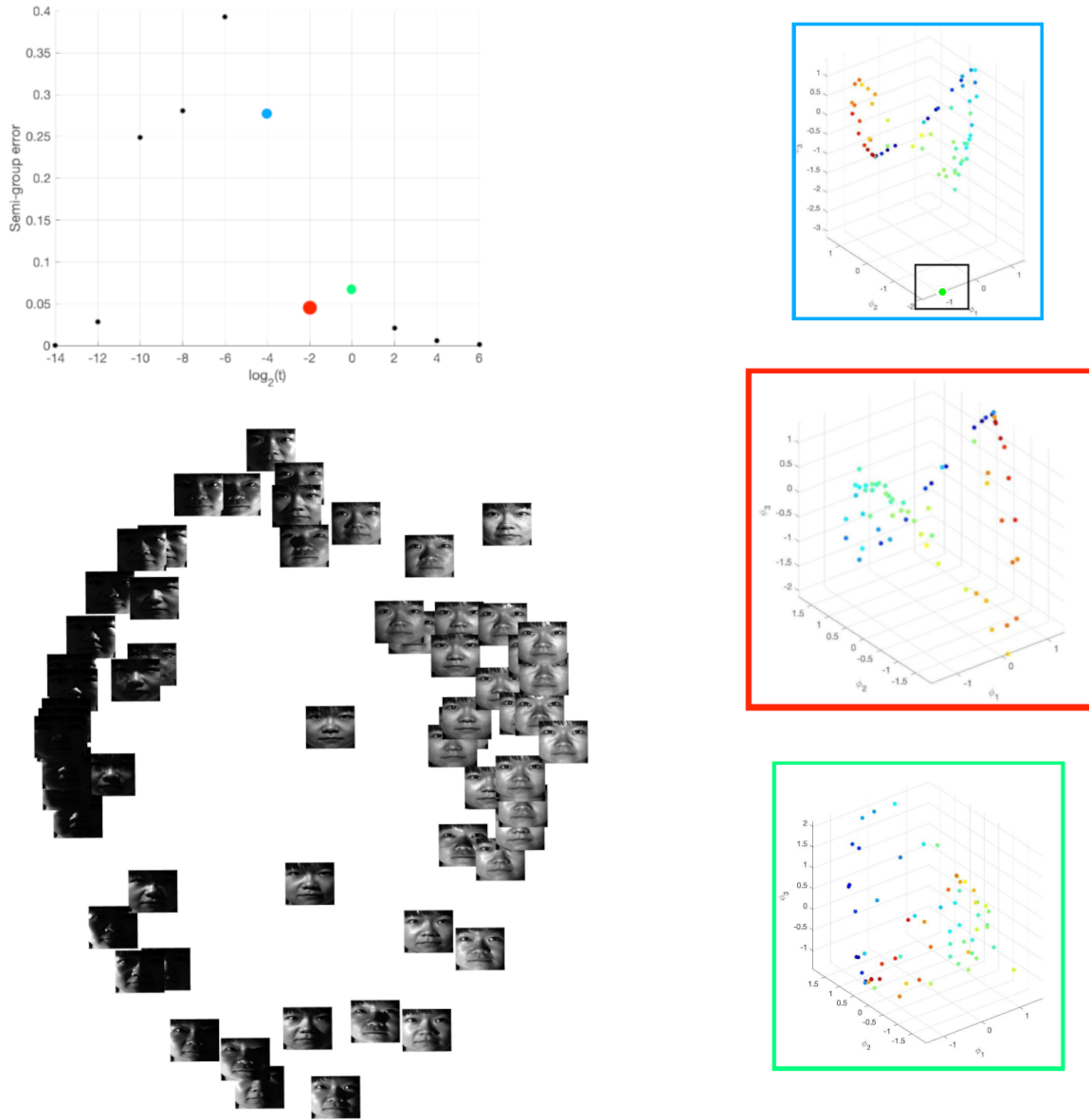


Figure 9: DM with the semigroup tuning strategy applied to the Yale Face dataset, in which each data point is an image of 192×168 pixels. Top left: $\text{SGE}(t)$ for a wide range of t . The colored boxes above show the embeddings using the first 3 non-trivial eigenvectors for the optimal choice $t_{\text{opt}} = 1/4$ and its two SGE-plot neighbors $t_{-4} = t_{\text{opt}}/4$ and $t_0 = 4 t_{\text{opt}}$. Although the embedding for t_{-4} looks comparable to that for t_{opt} at first sight, the embedding shows that one data point is not integrated well with the rest (boxed green datapoint near one of the axes); for t_0 the structure of the dataset is much less well-defined than for t_{opt} . Left: 2-dimensional DM embedding for t_{opt} , with the datapoints indicated by thumbprints of the images, indicating that the DM parametrization captured the illumination degrees of freedom in the dataset. (In this case, we set $\alpha = 1.5$ to determine the adapted kernels.)

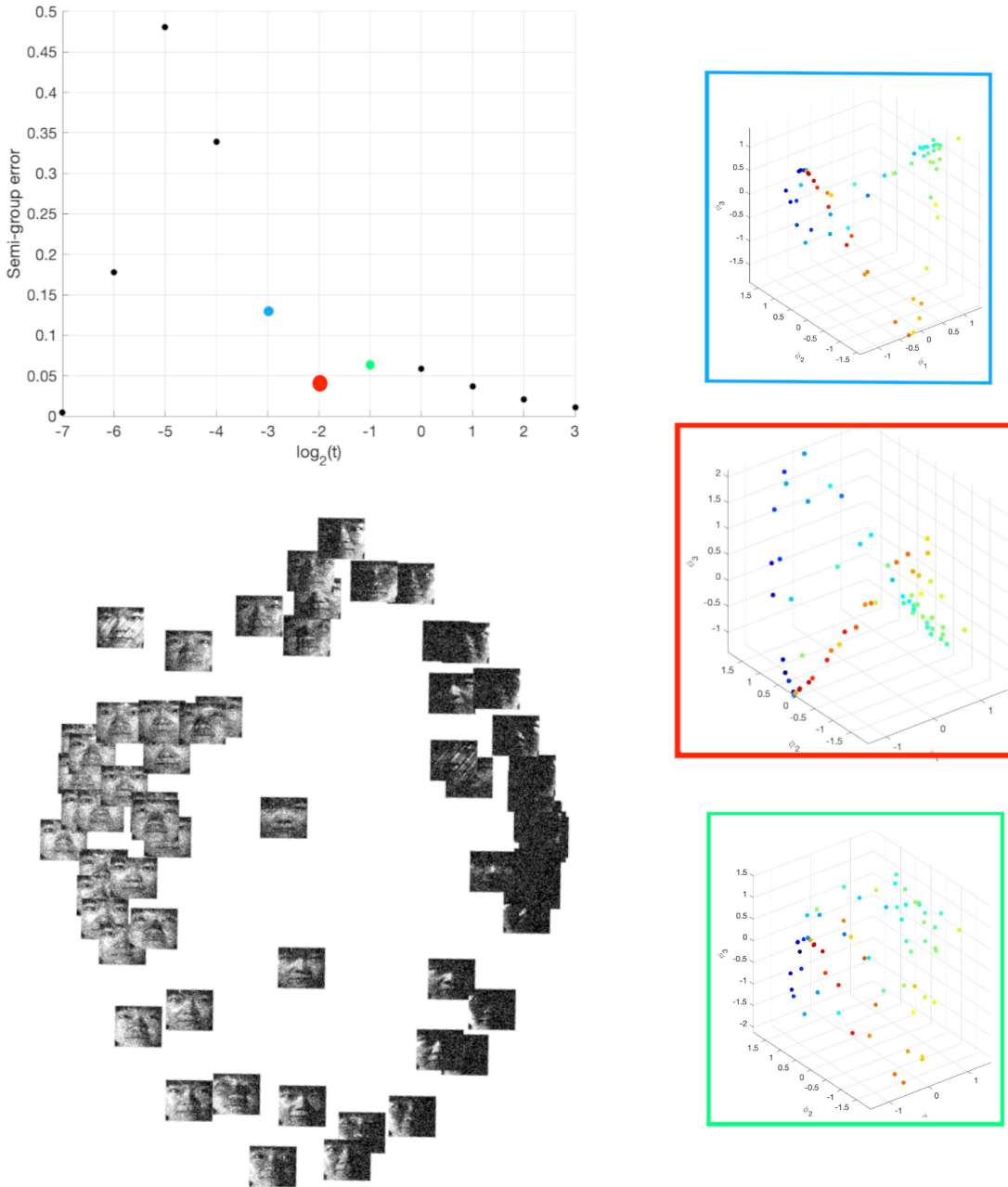


Figure 10: DM with the semigroup tuning strategy applied to the same Yale Face dataset as in Figure 9, after additional noise was added to each image of 192×168 pixels, i.e. to each data point. (The nature of the noise is explained below and illustrated in Figure 11.) Top left: $\text{SGE}(t)$ for a wide range of t . The colored boxes above show the embeddings using the first 3 non-trivial eigenvectors for the optimal choice $t_{\text{opt}} = 1/4$ and its two SGE -plot neighbors $t_{-4} = t_{\text{opt}}/4$ and $t_0 = 4 t_{\text{opt}}$. Left: 2-dimensional DM embedding for t_{opt} , with the datapoints indicated by thumbprints of the images. (We again set $\alpha = 1.5$ to determine the adapted kernels.)

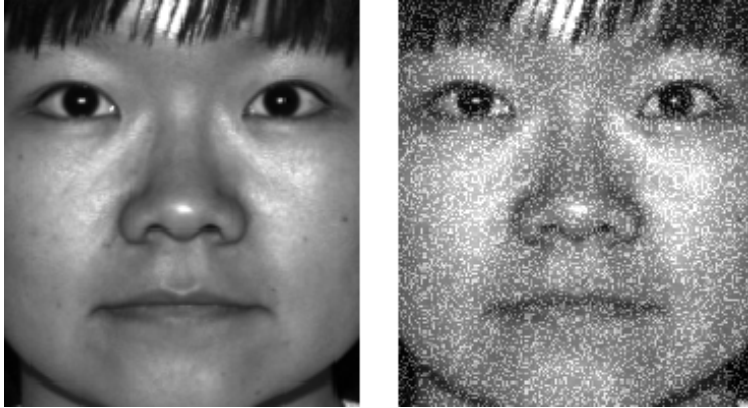


Figure 11: Left: one of the 64 images from the Yale Face dataset used in the analysis in Figure 9; Right: the noisy version of this image obtained by adding, pixelwise, random integers picked uniformly and independently in $[-100,100]$ to the gray value of the pixel, and rounding so the result is in $[0,225]$.



Figure 12: Left and Middle: the 2D embeddings from Figures 9 and 10, respectively, for the 64-face Yale Face dataset without and with the added noise illustrated in Figure 11. Up to a change of sign in the horizontal axis, the two embeddings are remarkably similar, as illustrated by the figure on the Right, which superimposes onto the Middle embedding a “skeleton” of the other embedding, indicating with a green rectangle the mirrored position of each thumbprint from the Left embedding. Closer scrutiny shows that thumbprints in close geometric proximity in this comparison picture do indeed correspond to the same face picture.